Atomic clusters in icosahedral *F*-type quasicrystals

Denis Gratias, Frédéric Puyraimond, and Marianne Quiquandon
LEM-CNRS/ONERA, BP 72, 29 Avenue de la division Leclerc, 92322 Châtillon Cedex, France

André Katz
Centre de Physique Théorique, Ecole Polytechnique 91128 Palaiseau Cedex, France
(Received 26 June 2000; published 18 December 2000)

We present a detailed study of the geometry of the atomic clusters encountered in icosahedral *F*-type quasicrystals using the cell decomposition of the prototypic atomic surfaces introduced several years ago for modeling *i*-AlCuFe. This includes an exhaustive and quantitative characterization of the geometrical features of the two major (Bergman- and Mackay-type) atomic clusters usually considered as the building blocks of these structures together with a study of the extended Bergman cluster proposed by M. Duneau (*Clusters in Quasicrystals*, to be published in the Proceedings of the 7th International Conference on Quasicrystals, Stuttgart, Sept. 1999) as a template of self-overlapping atomic clusters describing all atoms of the structure and show that this large cluster splits into a total of ten different configurations.

DOI: 10.1103/PhysRevB.63.024202 PACS number(s): 61.44.Br

I. INTRODUCTION

Stable icosahedral quasicrystals have been discovered by Tsai and co-workers[1,2] in the (Al,Cu,Fe) and (Al,Pd,Mn) ternary systems a few years after the observation of metastable icosahedral structures in rapidly quenched (Al,Mn) alloys by Shechtman *et al.*[3]. Extensive efforts have been since devoted to decipher the atomic structure of these phases by means of single grain x rays and neutron-diffraction technique (see, for instance, Refs. 4–7). Experimental results agree on the basic fact that these stable quasicrystals are well defined long-range-ordered solids with respect to Bragg diffraction (see, for instance, Refs. 8–12): the diffraction instruments with the best available resolution show that quasicrystals have a spatial coherent length close to that of standard silicon samples, thus ranking them among the best scatterering solids, far above the usual intermetallic compounds. This justifies describing quasicrystals, in a first approach, as perfect objects in the same spirit as describing perfect crystals. This is the ideal quasicrystal model that we take as the only focus of the present paper.

The present work is an additional contribution to previous works by Katz and Gratias,[13,15] Cockayne,[14] Elser,[16,17] Kramer *et al.*,[18] Papadopolos and co-workers,[19,20] and, more recently, Duneau[21] in the quantitative characterization of the geometrical features of the two major atomic clusters (Bergman and Mackay type) usually considered as the building blocks of these structures. We designate as atomic cluster a set of close atoms distributed on fully occupied high symmetry orbits and that can be considered as typical of the structure in the sense that they are found at a high frequency in the solid. This cluster idea was the aim of the pioneer works on quasicrystalline structures of Guyot and Audier[22] and Elser and Henley.[23] It gives a simple intuitive idea of what the quasicrystal looks like at atomic scale but it is, of course, a simplified view of the atomic structure of quasicrystals and if taken alone suffers severe deficiencies:

• it contains no information of how these units connect or overlap and how they develop quasiperiodically in space;

• a substantial fraction of atoms (often called the ''glue atoms'') are not taken into account although they are of a great importance for the understanding of the dynamical properties of the structure;

• none of the basic properties like density, composition, and diffraction spectra can be easily computed out of this simple picture;

• it gives the impression of a structure being frozen with unalterable atomic entities forming sort of an immutable molecular framework.

Because of these restrictions, we perform here a cluster analysis starting from the six-dimensional (6D) model proposed several years ago by two of us[15] for describing the atomic structure of *i*-AlCuFe. Our goal is twofold:

• quantitatively and exhaustively identify in details what type of atomic clusters develop with what frequency and how they connect and/or overlap;

• perform the complete decomposition of the three main atomic surfaces of the model into cells characteristic of each configuration for distributing the atomic species on the various sites of the clusters with respect to their local configurations consistently with quasiperiodicity.

The paper is organized as follows.

We first recall shortly the main physical and geometrical reasons for choosing the three main atomic surfaces that are the basis of our model and the cell decomposition technique that is used all along the paper for characterizing the real-space description. We then discuss the geometric properties of the two major kinds of generated atomic clusters similar to Bergman[24] and Mackay[25] clusters (noted, respectively, *B* and *M*) before extending the analysis to the cluster template (noted *XB*) recently proposed by Duneau.[21] We finally show that this template cluster splits into ten different configurations of the standard canonical triacontahedron.

II. BASIC MODEL

We use the cut method,[26–36] for describing the atomic structure of quasicrystals. In that scheme, the structure is

represented by a periodic object in a $N>3$D space where atoms are defined by atomic surfaces (also called acceptance windows) periodically distributed through an N-dimensional lattice. For the case of the icosahedral *i*-AlCuFe and *i*-AlPdMn phases, this configurational space is of dimension 6 and the structure is described by an F-type (face-centered) lattice (subset of nodes of the primitive 6D lattice with the sum of indices even) and 6D space group $Fm35$ or $F235$. The atomic surfaces are 3D volumes aligned along a 3D subspace, called $\mathbf{E}_\perp$ that is perpendicular to the physical 3D subspace called $\mathbf{E}_\parallel$. The real 3D structure is obtained by cutting the 6D object by any 3D subspace parallel to $\mathbf{E}_\parallel$. Atoms are generated in $\mathbf{E}_\parallel$ at the 3D locations where the atomic surfaces intersect the cut subspace.

We use the 6D indexing scheme of Cahn *et al.*[37] and label the F-lattice nodes with respect to the underlying primitive 6D lattice. To define a rational node of the hyperlattice, we use the full notation of Cahn *et al.* in including the numbers N and M characteristics of the lengths of the projected 3D vectors in $\mathbf{E}_\parallel$ and $\mathbf{E}_\perp$: a 6D vector $x=[N,M]:(n_1,n_2,n_3,n_4,n_5,n_6)$ projects on $\mathbf{E}_\parallel$ and $\mathbf{E}_\perp$ as 3D vectors with lengths, respectively, $|x_\parallel|=A\mathcal{K}\sqrt{(N+M\tau)}$ and $|x_\perp|=A\mathcal{K}\sqrt{\tau(N\tau-M)}$ where $\mathcal{K}$ is a geometric constant $\mathcal{K}=1/\sqrt{2(2+\tau)}(\approx 0.371\,748)$ and A is the 6D *primitive* lattice parameter.

A convenient and simple model[15] for F-type icosahedral phases consists in choosing three main atomic surfaces bounded by mirror planes:

(i) one attached to the even nodes $n=(0,0,0,0,0,0)$;

(ii) a second attached to the odd nodes $n'=(1,0,0,0,0,0)$;

(iii) a third one at the odd body centers $bc=1/2(-1,1,1,1,1,-1)$.

The three atomic surfaces that agree well with the diffraction data, density, and stoichiometry[8,10,15] are a large triacontahedron T_n at the even nodes n, a truncated (to avoid short distances with the former) triacontahedron $T_{n'}$ of same radius at the odd nodes n', and a small triacontahedron T_{bc} at the odd bodycenters (see Fig. 1). This choice fulfills the condition of existence of local rules[38–43] and easy phason relaxation[44–47] during growth (see, for instance, a discussion in Ref. 48).

We characterize the polyhedral atomic surfaces by a set of triangular facets in the elementary sector of the icosahedral symmetry. Each triangle is defined by three vectors in $\mathbf{E}_\perp$ that are projections of rational 6D lattice nodes. For example, the triacontahedron T_n is defined by one facet that is the perpendicular projection of the three 6D nodes $a=[7,-4]:(-1,-1,1,1,3,1)/2$, $b=[5,-3]:(0,-2,1,0,2,1)/2$ and $c=[6,-3]:(0,-1,1,0,1,0)$. For the unit lengths in $\mathbf{E}_\perp$ and $\mathbf{E}_\parallel$, we choose the triacontahedron T_{bc} as the unit volume in $\mathbf{E}_\perp$ and $\mathcal{K}A$ as the unit length in $\mathbf{E}_\parallel$. This gives a normalized description of the icosahedral phases independent on the chemical nature of the alloy. With these notations, the 3D Penrose canonical triacontahedron has volume $3+2\tau$ and, for the present model, T_n has volume $5+8\tau$, $T_{n'}$ $5+6\tau$, and T_{bc}, of course, 1. The total volume of the model is $11+14\tau$.

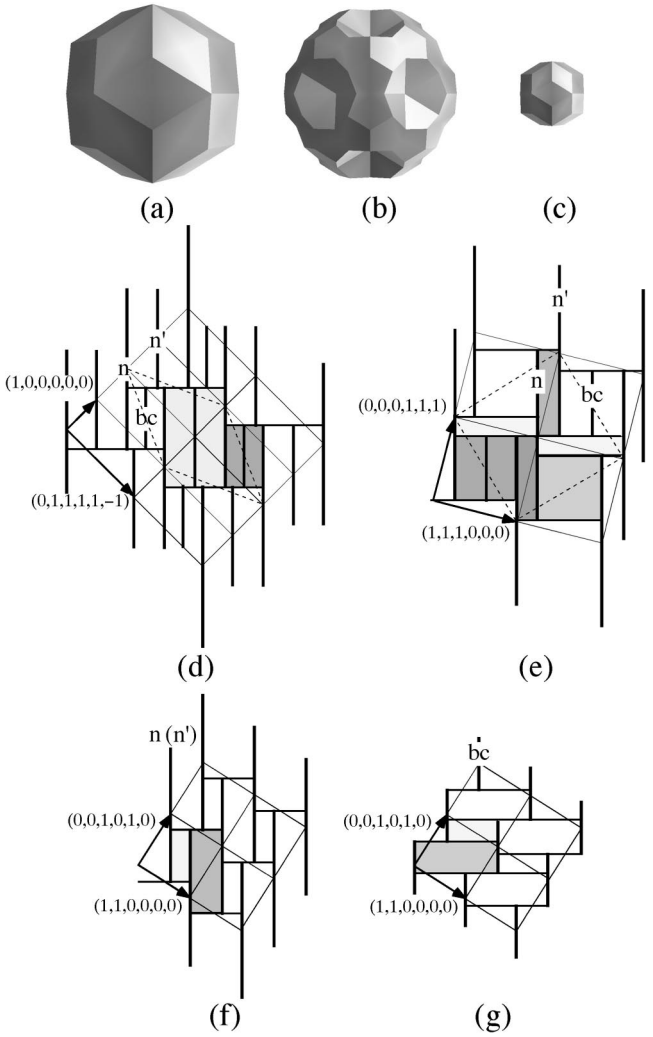

FIG. 1. (top) The three main atomic surfaces of the model in $\mathbf{E}_\perp$: (a) a large triacontahedron T_n of volume $5+8\tau$ located at $n=(0,0,0,0,0,0)$, (b) a large truncated triacontahedron $T_{n'}$ of volume $5+6\tau$ located at $n'=(1,0,0,0,0,0)$, and (c) a small triacontahedron T_{bc} of volume 1 located at $bc=(-1,1,1,1,1,-1)/2$. The total volume of the atomic surfaces is $11+14\tau$ leading to a density of sites d in real space of $d(\mathcal{K}A)^3=(11+14\tau)/[4(3+4\tau)]\approx 0.8882$. (bottom) 2D cut of the 6D space along (d) fivefold, (e) threefold, and (f), (g) twofold planes: the traces of the three basic polyhedra representing the atomic surfaces are line segments parallel to $\mathbf{E}_\perp$. Completed with segments parallel to $\mathbf{E}_\parallel$, they represent 2D sections of the 6D hyperprisms defining the cell decomposition. The gray areas represent the cut of the hyperprisms corresponding to the unit 6D cell.

III. ATOMIC CLUSTERS

The F-type icosahedral phases are often designated as ''Mackay-type'' structures (see for instance, Ref. 49) as opposed to ''Bergman-type'' structures like AlLiCu (see, for instance, Refs. 50 and 51). As already discussed by Katz and Gratias,[13] Elser,[16], Kramer *et al.*,[18] and Papadopolos and co-workers,[19,20] these structures can be (roughly) described by two kinds of intricated clusters that are reminiscent of Bergman's (designated here by B clusters) and Mackay's clusters (designated here by M clusters). Our aim is to fully

TABLE I. The principal short interatomic distances and their origins in 6D space. The parallel and perpendicular distances $d_\parallel$ and $d_\perp$ are given in nm for the specific case of AlCuFe calculated with a 6D-lattice parameter $A=0.63146$ nm (multiply by 1.0357 for *i*-AlPdMn).

Type	Sym (lattice)	6D vector	$d_\parallel$(nm)	$d_\perp$(nm)
$n-n'$	20(P)	[6,−3]:(1,0,0,−1,−1,0)	0.251286	1.06446
$n-bc$	12(I)	[3,−1]:(1,1,−1,1,−1,1)/2	0.275958	0.722468
$n-n$	30(F)	[8,−4]:(0,−1,1,0,1,1)	0.29016	1.22914
$n-n'$	60(P)	[14,−7]:(1,0,−1,1,0,2)	0.383845	1.62599
$n'-bc$	20(I)	[3,0]:(−1,1,1,1,1,1)/2	0.406589	0.657874
$n-n'$	12(P)	[2,1]:(0,0,1,0,0,0)	0.44651	0.44651
$n-n$	30(F)	[4,0]:(0,1,0,0,−1,0)	0.469488	0.759648
$n-bc$	60(I)	[7,−1]:(1,−1,1,1,1,3)/2	0.544584	1.04834
$n-n$	12(F)	[12,−4]:(1,1,−1,1,−1,1)	0.551916	1.44494
$n-n$	60(F)	[12,−4]:(−1,0,2,0,1,0)	0.551916	1.44494
$n'-bc$	60(I)	[7,0]:(−1,1,3,−1,−1,−1)/2	0.621074	1.00492
$n-n'$	60(P)	[6,1]:(0,1,0,1,0,1)	0.647912	0.881156
$n-bc$	20(I)	[3,3]:(1,1,1,−1,−1,1)/2	0.657874	0.406589
$n-n$	60(F)	[8,0]:(1,0,1,−1,−1,0)	0.663956	1.0743
$n'-bc$	12(I)	[3,4]:(1,1,1,1,−1,1)/2	0.722468	0.275958
$n-n$	30(F)	[4,4]:(0,0,1,0,0,1)	0.759648	0.469488
$n'-bc$	120(I)	[11,0]:(3,−1,1,−1,−1,3)/2	0.778558	1.25973
$n-n'$	60(P)	[10,1]:(0,0,2,−1,0,0)	0.800131	1.1634
$n-bc$	60(I)	[7,3]:(−1,1,3,1,1,1)/2	0.808219	0.861614
$n-n$	60(F)	[12,0]:(1,0,0,1,0,2)	0.813177	1.31575
$n-n$	20(F)	[12,0]:(−1,1,1,1,1,1)	0.813177	1.31575
$n'-bc$	60(I)	[7,4]:(−1,3,1,1,−1,1)/2	0.861614	0.808219
$n-n'$	60(P)	[6,5]:(0,1,1,0,−1,0)	0.881156	0.647912
$n-n$	12(F)	[8,4]:(0,0,2,0,0,0)	0.893019	0.893019
$n-n$	60(F)	[8,4]:(1,1,0,0,−1,1)	0.893019	0.893019
$n-n'$	120(P)	[14,1]:(0,0,1,1,1,2)	0.9277	1.38945
$n-bc$	60(I)	[11,3]:(3,1,1,−1,−3,1)/2	0.934685	1.14867
$n-bc$	60(I)	[11,3]:(1,−1,3,−1,1,3)/2	0.934685	1.14867
$n-n$	120(F)	[16,0]:(1,−1,2,−1,0,1)	0.938976	1.5193
$n-n$	30(F)	[16,0]:(0,2,0,0,−2,0)	0.938976	1.5193
$n'-bc$	60(I)	[11,4]:(1,−1,3,1,1,3)/2	0.981223	1.10918
$n-n'$	60(P)	[10,5]:(1,0,1,−1,−1,1)	0.998426	0.998426
$n-n'$	12(P)	[10,5]:(1,1,0,1,−1,1)	0.998426	0.998426
$n-bc$	60(I)	[7,7]:(1,1,1,1,−1,3)/2	1.00492	0.621074

quantify the relative frequencies of these clusters and classify their intersections using our previous model as basic generator for the cut method. Instead of generating any portion of the quasicrystal with arbitrary size using the cut algorithm, we should analyze the atomic local configurations directly in $\mathbf{E}_\perp$ where all the geometrical environments have a finite-size image that can be calculated exactly. This is the cell[52] or Klötze[53,54] decomposition that is based on the simple idea that *two actually present atoms in the structure are issued from two atomic surfaces the projection in* $\mathbf{E}_\perp$ *of which have a non empty intersection*. Thus we study how atomic surfaces projected in $\mathbf{E}_\perp$ intersect each others suffices to determine what kind of clusters are present in the real structure. This work is considerably simplified by the fact that the main first interatomic distances (see Table I) are along three-, five-, and two-fold directions. Hence we can draw the traces (lines) of the atomic surfaces in the five-, three-, and twofold 2D planes of the 6D space as shown in Fig. 1 and directly visualize the basic intersections between neighbor atomic surfaces.

A. First coordination shell

As shown on Table I and Fig.1, the three first atomic distances are, respectively, $R_3=\sqrt{6-3\tau}$ along the threefold directions (dodecahedron of radius 0.251 nm for *i*-AlCuFe), $R_5=\sqrt{3-\tau}$ along the fivefold directions (icosahedron of radius 0.275 nm for *i*-AlCuFe), and finally $R_2=\sqrt{8-4\tau}$ along the twofold directions (icosidodecahedron of radius 0.290 nm for *i*-AlCuFe). The next distance is much farther away ($\sqrt{14-7\tau}$ in mirror planes) so that these three first distances, being close to each other, can reasonably be considered as the first coordination shell.

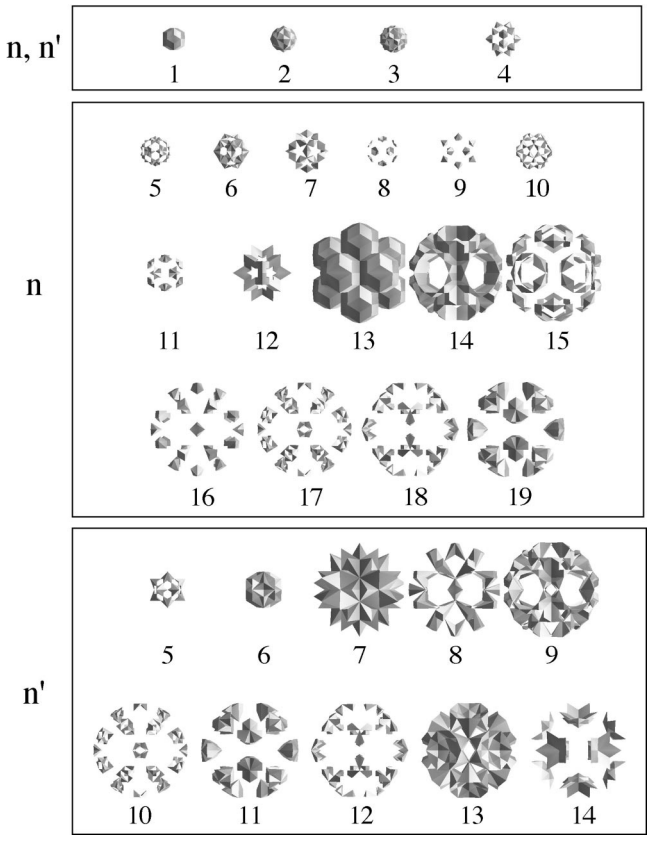

FIG. 2. First neighbor cell decomposition for T_n and $T_{n'}$ (see Tables II and III). The four first cells are common to T_n and $T_{n'}$.

The computation[13] of the corresponding cells decomposition leads to a total of 34 local configurations distributed according to 19 for T_n, 14 for $T_{n'}$ as shown on Fig. 2 and only one for T_{bc} (not shown). The characteristic environments along three-, five-, and twofold directions are given in Tables II and III.

The first coordination shell for T_n decomposes according to

- $\overline{Z}_n^{(3)}=(32+36\tau)/(5+8\tau)\approx 5.03$ average atoms along the threefold directions at R_3,
- $\overline{Z}_n^{(5)}=12/(5+8\tau)\approx 0.67$ average atoms along the fivefold directions at R_5,
- and $\overline{Z}_n^{(2)}=(32+52\tau)/(5+8\tau)=4\tau\approx 6.47$ average atoms along the twofold directions at R_2.

For $T_{n'}$, we obtain

- $\overline{Z}_{n'}^{(3)}=(32+36\tau)/(5+6\tau)\approx 6.136$ atoms along the threefold directions at R_3
- and $\overline{Z}_{n'}^{(2)}=(38+24\tau)/(5+6\tau)\approx 5.224$ atoms along the twofold directions at R_2.

Finally, for T_{bc}, we find $\overline{Z}_{bc}=12$ atoms along the fivefold directions (a full icosahedron) at R_5.

The average coordination numbers for each atomic surface are $\overline{Z}_n=(76+88\tau)/(5+8\tau)\approx 12.17$ for T_n, $\overline{Z}_{n'}=(70+60\tau)/(5+6\tau)\approx 11.36$ for $T_{n'}$, and, of course, $\overline{Z}_{bc}=12$ for T_{bc}. This leads to a total average coordination number of $\overline{Z}_T=(158+148\tau)/(11+14\tau)\approx 11.81$.

TABLE II. The coordination numbers Z for the first coordination shell decomposition of T_n (see Fig. 2). The average coordination number is $\overline{Z}_n=(76+88\tau)/(5+8\tau)\approx 12.17$.

Cell	Volume	Total at. %	Z (threefold)	Z (fivefold)	Z (twofold)	Z total
C_1	$-3+2\tau$	0.701	7	0	0	7
C_2	$13-8\tau$	0.1656	7	0	1	8
C_3	$-42+26\tau$	0.2047	7	0	2	9
C_4	$26-16\tau$	0.3312	7	0	3	10
C_5	$68-42\tau$	0.1265	7	0	3	10
C_6	$-42+26\tau$	0.2047	7	0	4	11
C_7	$-16+10\tau$	0.5359	7	0	5	12
C_8	$-55+34\tau$	0.0391	6	0	4	10
C_9	$13-8\tau$	0.1656	5	1	5	11
C_{10}	$13-8\tau$	0.1656	6	0	5	11
C_{11}	$13-8\tau$	0.1656	5	1	6	12
C_{12}	$36-22\tau$	1.1983	6	0	6	12
C_{13}	$-14+16\tau$	**35.327**	5	1	7	13
C_{14}	$8-4\tau$	4.5401	5	0	6	11
C_{15}	$-6+4\tau$	1.403	5	0	7	12
C_{16}	$7-4\tau$	1.5685	6	0	5	11
C_{17}	$-16+10\tau$	0.5359	5	0	5	10
C_{18}	$10-6\tau$	0.867	4	0	5	9
C_{19}	$-8+6\tau$	5.076	4	0	6	10

The average radii of the first coordination shells are $\overline{R}_n=[(32+36\tau)R_3+12R_5+(32+52\tau)R_2]/(76+88\tau)$ for T_n, $\overline{R}_{n'}=[(32+36\tau)R_3+(38+24\tau)R_2]/(70+60\tau)$ and, of course $\overline{R}_{bc}=\sqrt{3-\tau}$. The global average radius is $\overline{R}=0.2756$ nm for *i*-AlCuFe (0.2854 nm for *i*-AlPdMn). These values are much closer to those usually encountered in simple fcc metals (for instance, in aluminum $Z=12$, $\overline{R}_{Al}=0.28$ nm) than those encountered in amorphous metals or semiconductors: the present model is a compact structure.

TABLE III. The coordination numbers Z for the first coordination shell decomposition of $T_{n'}$ (see Fig. 2). The average coordination number for $T_{n'}$ is $\overline{Z}_{n'}=(70+60\tau)/(5+6\tau)\approx 11.36$.

Cell	Volume	Total at. %	Z(threfold)	Z(twofold)	Z total
C'_1	$-3+2\tau$	0.701	7	0	7
C'_2	$13-8\tau$	0.1656	7	1	8
C'_3	$-42+26\tau$	0.2047	7	2	9
C'_4	$26-16\tau$	0.3312	7	3	10
C'_5	$26-16\tau$	0.3312	7	3	10
C'_6	$-16+10\tau$	0.5359	7	4	11
C'_7	4τ	**19.2323**	7	5	12
C'_8	1	2.9715	6	5	11
C'_9	$14-8\tau$	3.137	5	6	11
C'_{10}	$-16+10\tau$	0.5359	5	5	10
C'_{11}	$-8+6\tau$	5.076	4	6	10
C'_{12}	$10-6\tau$	0.867	4	5	9
C'_{13}	$-6+4\tau$	1.403	6	5	11
C'_{14}	$6-2\tau$	8.213	6	6	12

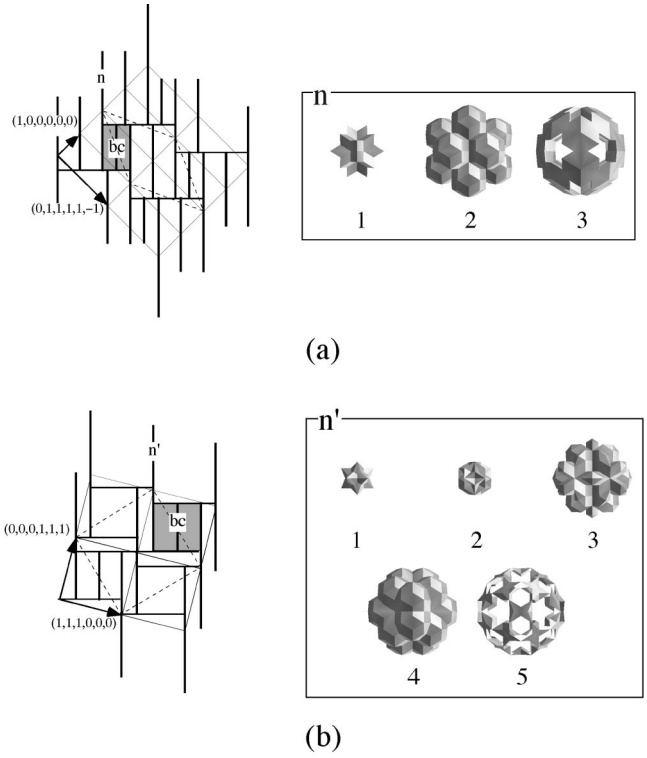

FIG. 3. *B*-cluster cell decomposition and associated volumes (see Table IV). (a) the atomic surface T_{bc} located at $[3,-1]$:(1,1,-1,1,-1,1)/2 (fivefold direction) projected onto T_n. The cell C_2 corresponds to the twelve T_{bc} that fall inside T_n generating the *B*-icosahedron in $\mathbf{E}_\parallel$; (b) the atomic surface T_{bc} located at [3,0]: $(-1,1,1,1,1,1)/2$ (threefold direction) onto $T_{n'}$. The cells C_2', C_3', and C_4' correspond to the 20 T_{bc} falling inside $T_{n'}$ thus generating the *B* dodecahedron in $\mathbf{E}_\parallel$.

As shown on Fig. 2, there are only three cells with full icosahedral symmetry: a small triacontahedron T_0 (cells C_1 and C_1' in Tables II and III) of volume $2\tau-3$, centered at n and n' and T_{bc} (volume 1) that forms a unique cell by itself. Studying these three cells leads us to decipher which kind of high-symmetry atomic clusters are present in the structure and how they distribute in space with respect to each other, as will be discussed next.

B. *B* clusters generated by T_{bc}

We characterize the body center configuration by projecting together in $\mathbf{E}_\perp$, T_{bc}, and the nearby atomic surfaces along two-, three-, and fivefold directions. The global decomposition is shown on Fig. 3 and Table IV. We first observe from Fig. 1 that there are no perpendicular projections of T_{bc} that intersect along the twofold direction at short distances. On the contrary, the projection in $\mathbf{E}_\perp$ of T_{bc} translated by $[3,-1]$:(1,1,-1,1,-1,1)/2 in a fivefold direction with respect to T_n falls entirely into the projection of T_n: if $\mathbf{E}_\parallel$ passes through T_{bc}, it *necessarily* passes through T_n and all other polyhedra of the same orbit around bc. This makes a total of 12 intersections defining 12 atomic sites surrounding the central site issued from T_{bc}. They form a complete icosahedron of radius R_5 (0.275 nm for AlCuFe). We designate this 13-atom cluster a *B* icosahedron. Conversely, looking at T_n (see Fig. 3), we see that 12 atomic surfaces T_{bc} fall inside T_n and adjust each other with no overlap. Therefore any point of T_n inside one of these small triacontahedra generates a site in $\mathbf{E}_\parallel$ that belongs to *one and only one B* icosahedron: the *B* icosahedra do not overlap. The fraction of T_n sites which are taken into account in the *B* icosahedron is given by the ratio of the volumes of the 12 T_{bc} divided by the volume of T_n, i.e. $12/(8\tau+5)\approx 66.87\%$: two-thirds of the T_n sites belong to a *B* icosahedron.

TABLE IV. *B*-cluster basic decomposition on T_n and $T_{n'}$ (see Fig. 3) and correspondence with Elser's notations. The cell C_5' corresponds to a fraction only of the M_2 sites of frequency $(-12+8\tau)$ suggested by Elser (see discussion).

Cell	Elser notations	Volume	Total at. %
On T_n	(n_1)		
C_1	P	$-2+2\tau$	3.67304
C_2	B_5	12	35.6586
C_3	M_3	$-5+6\tau$	13.9907
On $T_{n'}$	(n_0)		
C_1'	M_0	$-6+4\tau$	1.40298
C_2'	B_3 unshared	$10-6\tau$	0.867086
C_3'	B_3 shared	4τ	19.2323
C_4'	B_3 unshared	$10-2\tau$	20.0994
C_5'	M_2^*	$-9+6\tau$	2.10446

None of the two other distances of the first neighbor coordination shell lead to possible intersections. The next distance around a bc site is along the threefold directions at $[3,0]$:$(-1,1,1,1,1,1)/2$ corresponding, in $\mathbf{E}_\parallel$, to a dodecahedron of radius $\sqrt{3}$ (0.406 nm for *i*-AlCuFe). Here again, we observe that T_{bc} falls entirely inside $T_{n'}$. Each bc site is surrounded by a complete dodecahedron that we designate as a *B* dodecahedron. However, contrary to the previous case, the T_{bc} polyhedra overlap each other by pairs. Their intersections are shown on Fig. 3 (cell C_3'): a certain fraction of $T_{n'}$ sites belong simultaneously to *two B* dodecahedra. To find how they are connected we consider the symmetry elements of any pair of interpenetrating T_{bc}'s. The symmetry group is mmm and share $2mm$ with $T_{n'}$. Hence the *B* dodecahedra are connected by *two* (the order of mmm in $2mm$ is 2) vertices forming an *edge* of the *B* dodecahedron. We designate by *B* dodecahedron(1) (B_3 unshared in Elser's notations) the vertices of the dodecahedron that belong to one only dodecahedron and by *B* dodecahedron(2) (B_3 shared in Elser's notations), those that belong to two adjacent ones.

The fraction of $T_{n'}$ sites which belong to one (at least) *B* dodecahedron is given by the volume of the union of the interpenetrating T_{bc}, i.e., $20-4\tau$ so that $(20-4\tau)/(6\tau+5)\approx 91.97\%$ of the $T_{n'}$ sites belong to a *B* dodecahedron. The fraction of $T_{n'}$ sites that form the connected edges between these *B* dodecahedra is given by the volume of the intersection two by two of the T_{bc} which is 4τ. Therefore $4\tau/(6\tau+5)\approx 47.84\%$ of the $T_{n'}$ sites are involved in the dodecahedron-dodecahedron connections.

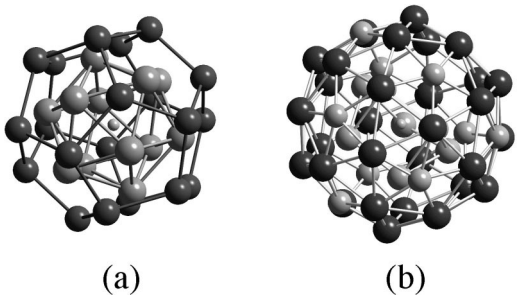

FIG. 4. (a) 33 atoms *B* cluster; (b) 50 atoms *M* cluster (the central dodecahedron contains only seven atoms). Observe that these two clusters are only similar to the Bergman and Mackay clusters encountered in several complex intermetallic phases.

Together, *B* icosahedra and *B* dodecahedra define a 33-atom cluster, shown in Fig. 4(a), that we call a *B* cluster as it is reminiscent of the Bergman polyhedron encountered in certain complex intermetallic phases. Each *bc* site of the real-space structure is the center of a *B* cluster.

The *B* clusters are connected together along twofold directions (icosidodecahedron) by [4,4](1,1,0,0,0,0) translations at distances $R=2\tau$ (0.759 nm for *i*-AlCuFe). The decomposition of T_{bc} by itself (see Fig. 5 and Table V) for this translation leads to 15 cells that are identical to those obtained for the first neighbors shell between two T_n's translated from each other by [8,−4](1,1,−1,0,−1,0) [compare Figs. 1(f) and (g)], but with an overall (linear) scaling factor of $2-\tau$ in $\mathbf{E}_\perp$ and $\tau+1$ in $\mathbf{E}_\parallel$. The average coordination number is $\overline{Z_B}=4\tau\approx 6.4721$. Hence the *B* clusters connect together in the same way as T_n atomic sites do, but with a length scale τ^2 larger.

As already noted by Elser[16,17] and Kramer *et al.*,[18] they distribute on the even nodes of a τ-scaled canonical 3D-Penrose tiling. When observed in Fig. 6 along a direction perpendicular to a fivefold direction, they appear as layers of three alternating thicknesses $L=A\sqrt{2}(\tau+1)/(\tau+2)$, L/τ and $S=L/\tau^2$ following a quasiperiodic sequence. This sequence can be generated by copying T_{bc} on the nodes of the 2D lattice defined by (5,−1,−1,−1,−1,1)/5 and (0,2,2,2,2,−2)/5 that results from the projection onto the fivefold 2D plane of the 6D structure. Each length appears with frequencies 1/2 for *M*, $(\tau-1)/2$ (30.9%) for *L* and $(2-\tau)/2$ (19.1%) for *S*. This feature is of greatest importance to understand the sequence in the terrace steps observed in scanning tunnel microscopy (STM) studies of quasicrystal surfaces.[20]

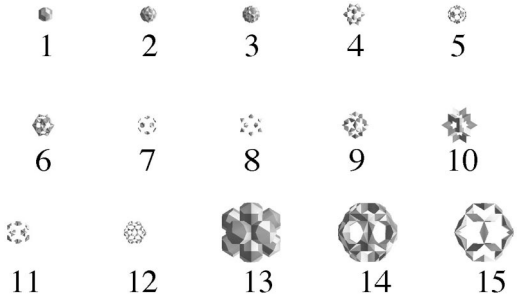

FIG. 5. Cell decomposition of T_{bc} by itself translated by [4,4](1,1,0,0,0,0) (see Table V). These 15 cells are directly calculated from those obtained by the first neighbors shell of two T_n displaced by [8,−4](1,1,−1,0,−1,0) and rescaling by $2-\tau$.

TABLE V. The coordination numbers Z_B for the *B* clusters network (see Figs. 5 and 6). The *B* clusters connect in $\mathbf{E}_\parallel$ only along twofold directions at distances $R=2$ from center to center and share an edge of the external dodecahedron. A small fraction (cell C_1) of 1.3155% of the *B* clusters have no connections with the others; they are the centers of (full) icosidodecahedra of radius $R=2\sqrt{2}$ of *B* clusters.

Cell	Volume	*B* cluster %	Z_B(twofold)
C_1	$-55+34\tau$	1.3155	0
C_2	$233-144\tau$	0.31056	1
C_3	$-754+466\tau$	0.38387	2
C_4	$466-288\tau$	0.6211	3
C_5	$1220-754\tau$	0.2372	3
C_6	$-754+466\tau$	0.38387	4
C_7	$-987+610\tau$	0.0733	4
C_8	$233-144\tau$	0.3106	5
C_9	$-288+178\tau$	1.005	5
C_{10}	$644-398\tau$	2.2472	6
C_{11}	$233-144\tau$	0.3106	6
C_{12}	$233-144\tau$	0.3106	5
C_{13}	$-420+260\tau$	**68.8837**	7
C_{14}	$-16+10\tau$	18.034	6
C_{15}	$13-8\tau$	5.5728	5

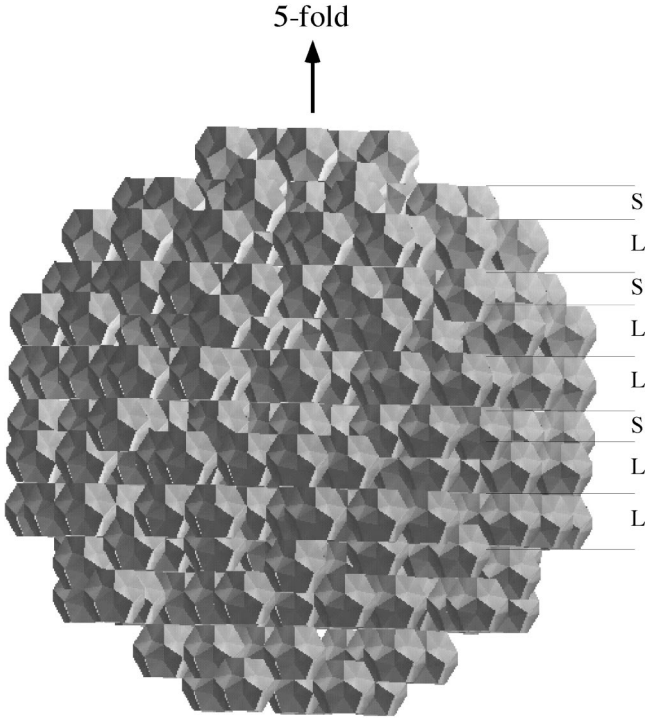

FIG. 6. *B* clusters network in $\mathbf{E}_\parallel$. These clusters are stacked in flat layers perpendicular to the fivefold directions of thickness $L=A\sqrt{2}(\tau+1)/(\tau+2)$, L/τ and $S=L/\tau^2$ distributed according to a Fibonacci-like sequence.

To compute how much of the atomic structure is described by the *B* clusters, we sum up all volumes that have been explored in constructing the cluster. These are the volume of T_{bc} (1) plus a volume of 12 in T_n and a volume of $20-4\tau$ in $T_{n'}$. Hence the total fraction of explored sites is $(1+12+20-4\tau)/(11+14\tau)\approx 78.83\%$ of the total number of sites in the structure.

C. *M* clusters generated by T_0 at *n*

Similarly to the previous section, we search for projections in $\mathbf{E}_\perp$ of the atomic surfaces that have a nonempty intersection with T_0 located at the even nodes.

From Fig. 1 and as shown in Fig. 7, we find a nonempty intersection between T_0 and $T_{n'}$ displaced by the threefold translation $[6,-3]$:(1,0,0,-1,-1,0) thus defining the *M* dodecahedron of radius R_3 (0.251 nm for *i*-AlCuFe). As shown on Fig. 7(a), this intersection is only partial: the 20 T_0 around n' give a total intersection volume of $7(2\tau-3)$ instead of $20(2\tau-3)$ if they would be fully embedded in $T_{n'}$. This means that the *M* dodecahedron of the coordination shell around an *n* site generated by T_0 is occupied by 7 atoms only over the 20 vertices of the dodecahedron. This is consistent with the fact that the edges of the dodecahedron have a too short length for being physically acceptable as interatomic distances (0.175 nm for *i*-AlCuFe). These seven atoms distribute on the dodecahedron such as never occupying simultaneously first neighbor sites and opposite sites. As shown by Lyonnard *et al.*,[55] there are 100 possibilities that group into two prototypes with respect to icosahedral symmetry, one with local symmetry 3 of multiplicity 40 and one with a mirror of multiplicity 60.

The next intersection corresponds to translating $T_{n'}$ by $[2,1]$:(0,0,1,0,0,0) along a fivefold direction, defining the *M*-icosahedron in $\mathbf{E}_\parallel$ of radius $\sqrt{2+\tau}$ (0.4465 nm for *i*-AlCuFe). As shown on Fig. 7(b) It leads to a full immersion of T_0 in $T_{n'}$, exactly like for the case of the full icosahedron of the *B* clusters but deflated by a factor τ. Node sites generated by T_0 have a full icosahedral shell issued from n' sites. Atoms on this *M* icosahedron belong to one and only one such shell.

The next nonempty intersection is found with T_n being translated along twofold direction by $[4,0]$:(0,1,0,0,-1,0) defining the *M* icosidodecahedron in $\mathbf{E}_\parallel$ of radius 2 (0.469 nm for *i*-AlCuFe). Here again [see Fig. 7(c)], T_0 is entirely contained into the projection of T_n thus leading to a fully occupied icosidodecahedron.

Together these shells form a cluster of 50 atoms[49] [see Fig. 4(b)], that we call a *M* cluster as it is reminiscent of the Mackay polyhedron. The fraction of atoms belonging to a *M* cluster is calculated by summing the volumes of the atomic surfaces that have been explored: $2\tau-3$ for the central atom, $7(2\tau-3)$ for the atoms of the partial dodecahedron, $12(2\tau-3)$ for the icosahedron, and $30(2\tau-3)$ for the icosidodecahedron: $50(2\tau-3)$. This represents a fraction of $50(2\tau-3)/(14\tau+11)\approx 35.0744\%$ of the atoms of the structure.

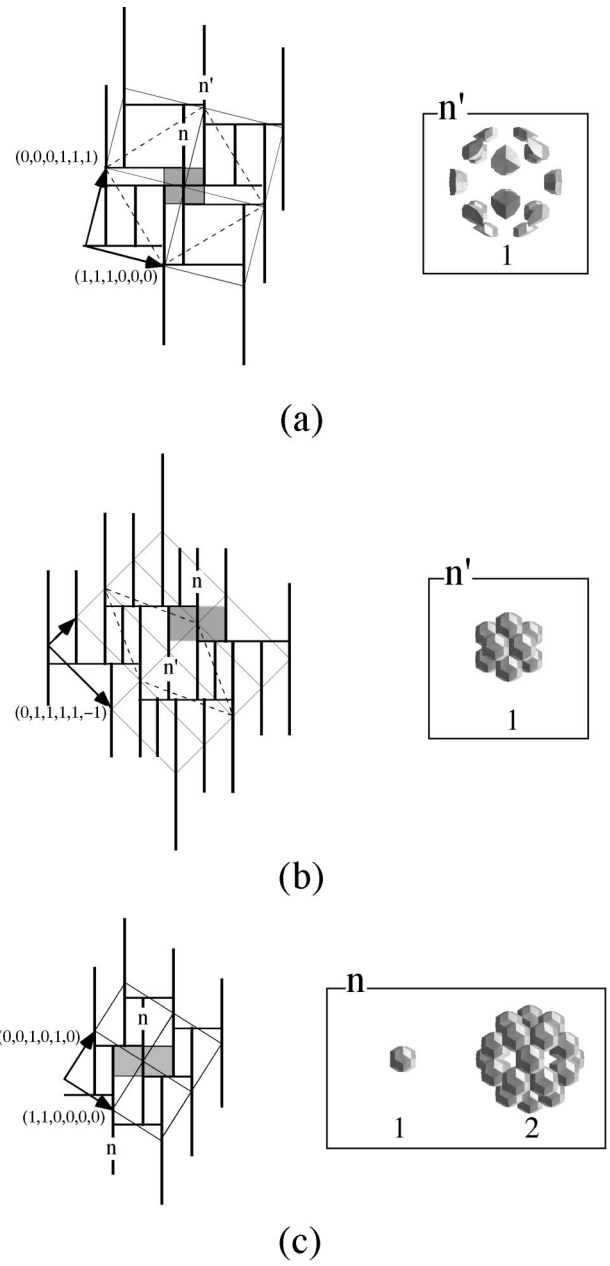

FIG. 7. *M*-clusters cell decomposition: the *M* cluster consists of seven atoms (a) among the 20 of a dodecahedron issued from the partial intersections of T_0 with the $T_{n'}$ atomic surfaces + 12 atoms, (b) on a full icosahedron issued from $T_{n'}$ atomic surfaces + 20 atoms, (c) on an icosidodecahedron issued from T_n and T_0 itself.

The *M* clusters are disconnected from each other but they significantly intersect with *B* clusters. This can be quantified by examining the intersections in $\mathbf{E}_\perp$ between the cells of the *B* clusters and those of the *M* clusters: all seven atoms of their inner dodecahedra are common to *B* dodecahedra, 11 atoms over 12 of the *M* icosahedra belong to *B* dodecahedra, and 21 atoms of the *M* icosidodecahedra belong to *B* icosahedra.

D. *M′* clusters generated by T_0 at n'

The very same analysis can be performed starting from T_0 located on n' instead of *n*. The decomposition leads to the

same polyhedra as those of the M clusters by exchanging n and n' leading to M' clusters identical to M clusters with respect to their geometry. They represent the same fraction of the atoms of the structure.

The crucial difference between M and M' clusters is the way they intersect with the B clusters.[17] The cells corresponding to the partially occupied inner dodecahedron [Fig. 7(a)] have empty intersection with the cells of the B clusters on n': the atoms of the M' dodecahedron do not belong to B clusters. On the contrary, eight atoms among 12 of the M' icosahedra belong to B clusters. The atoms of the M' icosidodecahedron distribute according to: $16-2\tau$ (≈ 12.7639) being common to a B dodecahedron on sites that are not linking two B clusters and $19-2\tau$ (≈ 15.7639) on sites that connect two B clusters. Finally only $-5+4\tau$ ($\approx 1.472\,14$) sites of the M' icosidodecahedra do not belong to B clusters. Hence most atoms of the M' icosidodecahedra are atoms of the B dodecahedra. Loosely speaking, the M' clusters can be seen as complementary to the B clusters.

Each of the two families M and M' clusters, taken alone, is a set of disconnected clusters. Together, they have intersections that can be analyzed as follows. The three basic cells of the decomposition shown in Fig. 7 have no intersection because the decomposition corresponding to the icosidodecahedron and the initial T_0 cells are on one atomic surface [Fig. 7(c)] and those corresponding to the icosahedron and the partial dodecahedron on the other [Figs. 7(a) and (b)]. Grouping the two families is equivalent to merging all cells on a same atomic surface T_n or $T_{n'}$. Then, some cells intersect and define new existence domains in $\mathbf{E}_\perp$ that correspond to sites that are common to both types of clusters. The cell T_0, corresponding to the centers of the M and M' clusters, intersect the cell corresponding to the outer icosahedra of, respectively, M' and M clusters, forming 12 small caps with volume $(34-21\tau)/6$ each. This, in turn, intersects the one of the cell corresponding to the icosidodecahedron of the other cluster in 60 identical small caps, which, finally, intersects the periphery cell of the partial dodecahedron, thus adding 60 new small caps to the common intersection. This leads to a total of $(12+60+60)=132$ intersections per atomic surface n and n' with a total volume of $2\times 132(34-21\tau)/6$ ($\approx 0.936\,59$): a small fraction of 2.78% of the atoms of the structure are common to M and M' clusters.

We observe that the $M(M')$ clusters generate cells that are scattered in the large atomic surfaces and interpenetrate into each other between M and M' cells (see Fig. 7). On the contrary, the B-clusters cells are very compact and describe a large portion of the atomic surfaces with an unique overlap on n' (see Fig. 3). This makes the terminology of Mackay-type structures, often used to designate the F-type icosahedral phases, somewhat questionable in front of the present geometrical analysis. The F-type structures can equally well be viewed—and even better with respect to compacity of the clusters, frequencies, connectivity, and cells geometry in $\mathbf{E}_\perp$—as a connected network of B clusters rather than accretion of $M(M')$ clusters.

E. *B, M, M′* cluster connections

As already mentioned, B clusters distribute on the even nodes of a 3D Penrose tiling scaled by τ. They intersect M clusters along the threefold directions according to four different configurations as shown on Fig. 8 and Table VI. The average number of intersecting M clusters is $\overline{Z}_M^B=5-2\tau$ (1.764) with a high frequency for the configuration with two M clusters intersecting a B cluster. The B clusters are connected to M' clusters (along fivefold directions) and share a full pentagonal face. The average number of adjacent M' clusters is $\overline{Z}_{M'}^B=-148+92\tau$ (0.859) and $36-22\tau$ (40.325%) of B clusters have no adjacent M' clusters.

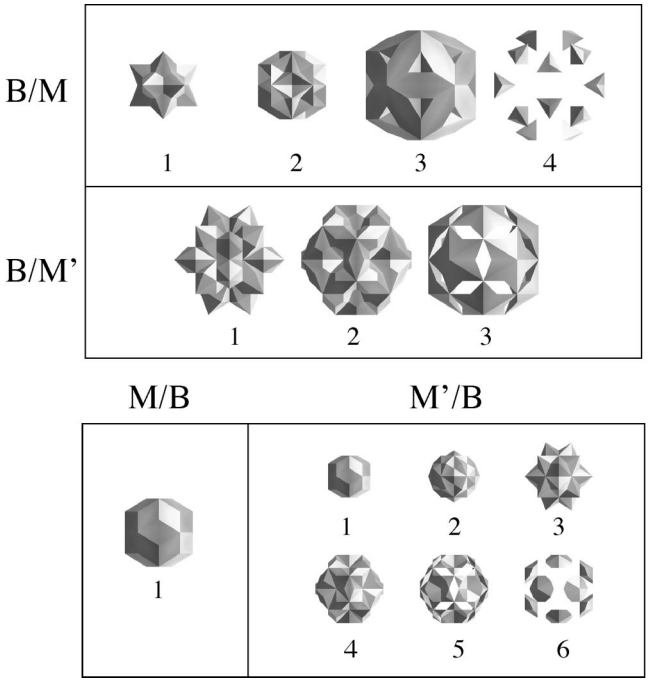

FIG. 8. Cell decomposition for B-/$M(M')$ clusters connections (see Table VI). On top: (upper line) the cells of the four configurations of M clusters around a B cluster, (lower line) the existence domains of the three configurations of M' clusters around a B cluster. On bottom: (left) the cell of the unique configuration of B clusters around an M cluster; (right) the cells of the six configurations of B clusters around an M' cluster.

The same analysis leads to M clusters having a unique configuration with $\overline{Z}_B^M=7$ intersecting B clusters distributed in the same way as the atoms of the M dodecahedron with the configuration of multiplicity 60 (mirror symmetry). This configuration corresponds to five B clusters distributed on a pentagon and two out of the plane (like a ''stone thrower''). The M' clusters distribute according to six configurations with an average number of $\overline{Z}_B^{M'}=12-2\tau$ (8.764) adjacent B clusters. As shown on Table VI, there are two major configurations with same frequency, one with 12 neighboring B clusters and the other with 8.

F. Complete *B, M,* and *M′* decomposition

We now analyze the three kinds of clusters together. This is achieved by computing the mutual intersections between

TABLE VI. The coordination numbers $Z_{M,M'}$ and Z_B corresponding to the local surrounding of B clusters by M (M') clusters and vice versa (see Fig. 8).

B/M cells	Volume	B-cluster %	Z_M^B(threefold)
C_1	$26-16\tau$	11.1456	0
C_2	$-42+26\tau$	6.89	1
C_3	$4-2\tau$	**76.39**	2
C_4	$13-8\tau$	5.573	3
B/M' cells	Volume	B-cluster %	$Z_{M'}^B$(fivefold)
C_1'	$36-22\tau$	**40.325**	0
C_2'	$-113+70\tau$	26.238	2
C_3'	$78-48\tau$	33.437	1
M/B cell	Volume	M-cluster %	Z_B^M(threefold)
C_1	$-3+2\tau$	**100**	7
M'/B cells	Volume	M'-cluster %	$Z_B^{M'}$(fivefold)
C_1'	$13-8\tau$	**23.607**	12
C_2'	$-55+34\tau$	5.573	10
C_3'	$68-42\tau$	18.034	9
C_4'	$13-8\tau$	**23.607**	8
C_5'	$-110+68\tau$	11.146	7
C_6'	$68-42\tau$	18.034	6

all the cells discussed in the previous sections. The results are given on Fig. 9 and Tables VII and VIII. The first column in these tables defines the cell number, the second column gives its volume which, divided by the total volume of the atomic surfaces gives, in the third column, the global concentration in at. % of the atoms generated by the cell. The last column gives a short description of the geometrical properties of the atoms generated by the cell with respect to the three clusters. For example, the cell C_7 on T_n generates atoms that simultaneously belong to a B icosahedron, a M icosidodecahedron, and a M' icosahedron; similarly, C_8' on $T_{n'}$ generates atoms that belong to two B dodecahedra (i.e., on the vertices of the pairs that link two B clusters), a M icosahedron and a M' icosidodecahedron. Both kinds of atomic sites represent a concentration of 0.6325% of the atoms of the structure.

Using Tables VII and VIII leads to a possible tailorization of the crystallochemistry of the three kinds of clusters. We can *ad libidum* decorate the cells for obtaining whatever cluster chemical decoration we wish in a way that is consistent with quasiperiodicity and overlaps.

Regrouping the cells associated to B and $M(M')$ clusters configurations leads to describing roughly 95% of the whole structure. The remaining cells C_3, C_5, and C_{11} on T_n and C_3', C_{16}', on $T_{n'}$ generate the so-called ''glue atoms'' that do not belong to either of the basic clusters. These cells have a total volume of $484-298\tau$ ($\approx 1.825\,87$). They are shown on the right side of Fig. 9. They are located at the periphery of

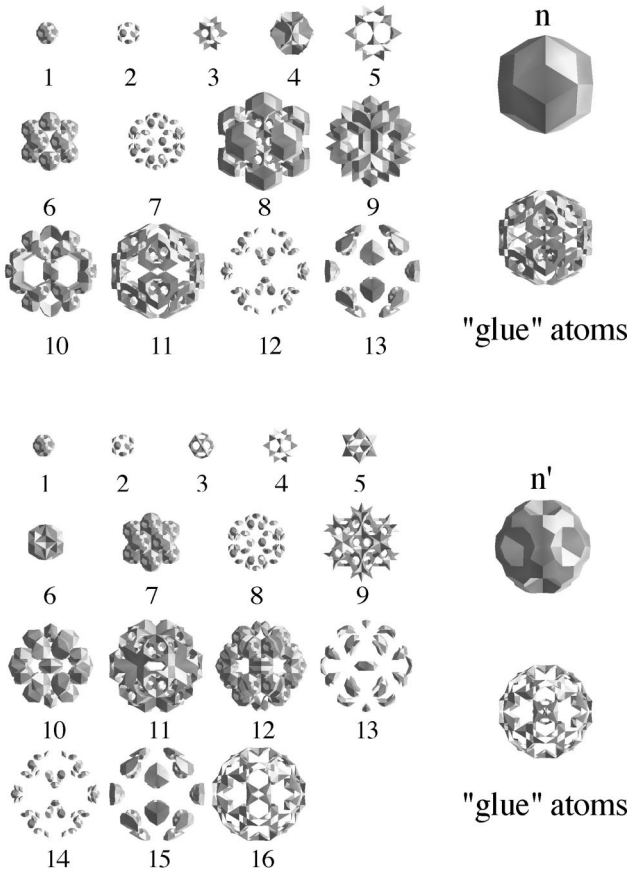

FIG. 9. Complete cell decomposition with B, M, and M' clusters (see Tables VII and VIII): (top) for T_n leading to 13 cells, (bottom) for $T_{n'}$ leading to 16 cells. On the right the existence domains of the ''glue'' atoms (atoms of the model that belong to none of these clusters).

the atomic surfaces and on intermediate internal regions surrounding the central cells. An example of the complete network of B, M, and M' clusters is shown on Fig. 10.

These ''glue'' atoms play a central role in the way the clusters rearrange under a translation of the cut in $\mathbf{E}_\perp$ as illustrated on Fig. 11. A translation in $\mathbf{E}_\perp$ passing through a boundary of an atomic surface changes the way the clusters connect. Most of the ''glue'' atoms form partial clusters that can be completed through a few atom jumps from the existing clusters. Those disappear to the benefit of the new ones. Hence the glue atoms are sort of ''transient sites,'' a reservoir for virtual clusters, and are very important in both the dynamics and the configurational entropy of the clusters that should be viewed, at high enough temperatures, as dynamical entities that form and deform through individual atom jumps. Because the cells defining the $M(M')$ clusters are smaller and more scattered in $\mathbf{E}_\perp$ than those corresponding to the B clusters, the average fluctuation dynamics of cluster rearrangement should be higher for the $M(M')$ clusters than for the B clusters. To that aspect, the B clusters could be considered as more ''stable'' than the $M(M')$ clusters.

TABLE VII. Complete cell decomposition (see Fig. 9) of T_n with respect to *B*, *M*, and M' clusters.

Cell	Volume	Total at. %	Type of environment
C_1	$-71+44\tau$	0.575	*M* center
C_2	$68-42\tau$	0.1265	*M* center + M' icosahedron
C_3	$81-50\tau$	0.2921	
C_4	$-64+40\tau$	2.1435	M' icosahedron
C_5	$-16+10\tau$	0.5359	
C_6	$-380+236\tau$	5.5153	*B* icosahedron + M' icosahedron
C_7	$340-210\tau$	0.6325	*B* icosahedron + *M* icosidodecahedron +M' icosahedron
C_8	$455-278\tau$	**15.42**	*B* icosahedron
C_9	$-403+252\tau$	**14.1**	*B* icosahedron + *M* icosidodecahedron
C_{10}	$-367+228\tau$	5.681	*M* icosidodecahedron
C_{11}	$383-236\tau$	3.399	
C_{12}	$340-210\tau$	0.6325	*M* icosidodecahedron + M' dodecahedron
C_{13}	$-361+224\tau$	4.278	M' dodecahedron

G. Extended *B* cluster (*XB*)

Duneau[21] recently proposed to extend the size of the clusters in a search for including all atoms of the model in a unique description. He showed that an economical extension is obtained from the *B* cluster by adding the four next distances around the *bc* sites (see Table IX), leading to a cluster, noted *XB* for short, with six shells shown in Fig. 12 and defined by

icosahedron: $bc-n$ at [3,-1]:(1,1,-1,1,-1,1)/2;

dodecahedron: $bc-n'$ at [3,0]:(-1,1,1,1,1,1)/2;

truncated icosahedron 1: (*TI*) (*): $bc-n$ at [7,-1]:(1,-1,1,1,1,3)/2;

truncated icosahedron 2: (TI') (*): $bc-n'$ at [7,0]:(-1,1,3,-1,-1,-1)/2;

triacontahedron: $bc-n$ at [3,3]:(1,1,1,-1,-1,1)/2 and $bc-n'$ at [3,4]:(1,1,1,1,-1,1)/2.

The two first shells correspond to the *B* cluster already discussed.

The two next shells, noted with (*), correspond to the orbits *TI* and TI' of multiplicity 60 that are *partially* occupied [as the inner dodecahedra of the $M(M')$ clusters] as shown on Fig. 13 and Tables X and XI. The average number of atoms is $\overline{Z_{TI}}=-15+24\tau$ (23.83) for *TI* and $\overline{Z_{TI'}}=181-98\tau$ (22.43) for TI' in agreement with Duneau's calculations[21] (except for TI' where Duneau finds 22.36 instead of 22.43 as found here). These two orbits have strong overlaps with the neighboring *B* clusters.

TABLE VIII. Complete cell decomposition (see Fig. 9) of $T_{n'}$ with respect to *B*, *M*, and M' clusters.

Cell	Volume	Total at. %	Type of environment
C'_1	$-71+44\tau$	0.575	M' center
C'_2	$68-42\tau$	0.1265	M' center + *M* icosahedron
C'_3	$658-42\tau$	0.1265	
C'_4	$13-8\tau$	0.1656	*B* dodecahedron(1)
C'_5	$-71+44\tau$	0.5750	*M* icosahedron
C'_6	$-3+2\tau$	0.7015	*B* dodecahedron(1) + *M* icosahedron
C'_7	$-370+230\tau$	6.382	*B* dodecahedron(2) + *M* icosahedron
C'_8	$340-210\tau$	0.6325	*B* dodecahedron(2) + *M* icosahedron +M' icosidodecahedron
C'_9	$457-282\tau$	2.123	*B* dodecahedron(2)
C'_{10}	$-427+266\tau$	**10.09**	*B* dodecahedron(2) + M' icosidodecahedron
C'_{11}	$397-244\tau$	6.5368	*B* dodecahedron(1)
C'_{12}	$-366+228\tau$	8.6524	*B* dodecahedron(1) + M' icosidodecahedron
C'_{13}	$23-14\tau$	1.033	M' icosidodecahedron
C'_{14}	$340-210\tau$	0.6325	*B* dodecahedron(1) + *M* dodecahedron +M' icosidodecahedron
C'_{15}	$-361+224\tau$	4.278	*B* dodecahedron(1) + *M* dodecahedron
C'_{16}	$-32+20\tau$	1.072	

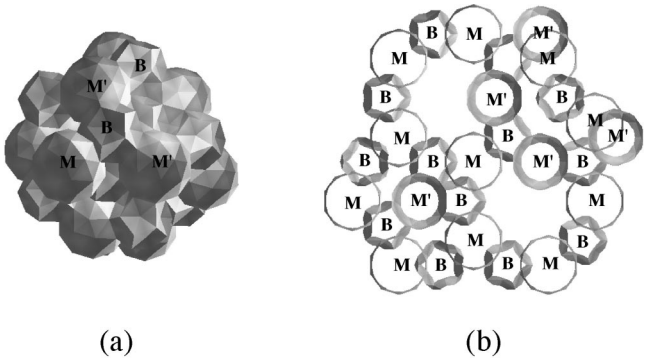

FIG. 10. (a) A portion of the full network of *B*, *M*, and *M'* clusters; (b) a typical slab of these clusters perpendicular to a fivefold axis showing how *M* and *M'* clusters intersect *B* clusters.

The orbit *TI* contains a fraction of 65.164% $[(12-5\tau)/6]$ of the atoms of the *B* icosahedra and *TI'* contains 70.02% $[(3+4\tau)/(20-4\tau)]$ of the atoms of the *B* dodecahedra. The orbit *TI* gives three different configurations with 22 to 24 atoms. The configuration C_1 corresponding to the maximum number of atoms (24) has by far the highest frequency (88.85% of the *XB* clusters). The atoms of the *TI* of a given *XB* cluster belong in average simultaneously to 1.88 others $[(-25+30\tau)/(19-4\tau)]$. They represent a fraction of 69.81% $[(19-4\tau)/(5+8\tau)]$ of the atoms generated by T_n.

The orbit *TI'* gives six different configurations with 20 to 23 atoms (see Fig. 13 and Tables X and XI). Here also, the configuration C_1', corresponding to the maximum number of atoms has the highest frequency (65.25%). Atoms of *TI'* of a given *XB* cluster belong in average to 2.19 others $[(-10+20\tau)/(-6+10\tau)]$. They represent a fraction of 69.21% $[(-6+10\tau)/(5+6\tau)]$ of the atoms generated by $T_{n'}$.

The last shell—containing a fivefold and a threefold orbit—is the canonical triacontahedron of the primitive Penrose 3D and is fully occupied (32 atoms). The corresponding decomposition is shown on Table XII and Fig. 14. It overlaps with the neighboring *B* clusters in the following way.

The threefold orbit of the triacontahedron contains 46.06% $[(3-\tau)/3]$ of the atoms of the *B* icosahedra and the fivefold orbit contains 26.49% $[(23-12\tau)/(20-4\tau)]$ of those of the *B* dodecahedra. The T_n is decomposed into 12 cells [see Fig. 14(a)] by the threefold orbit, the last one, C_{12}, corresponding to atoms that do not belong to any triacontahedron of the *XB* cluster. Hence a fraction of 39.32% $[(20-8\tau)/(5+8\tau)]$ of the atoms generated by T_n belong to at least one triacontahedron. Each of these atoms belongs to 2.736 $[(-26+28\tau)/(20-8\tau)]$ *XB* clusters in average. Also, 10.45% $[(31-18\tau)/(5+6\tau)]$ of the atoms generated by T_n belong simultaneously to a *TI* and a threefold orbit of the triacontahedron.

The fivefold orbit splits $T_{n'}$ into 13 cells, the last one (C_{13}') corresponding to atoms that do not belong to any triacontahedron of the *XB* cluster. The atoms of the fivefold orbit represent 27.57% $[(17-18\tau)/(5+6\tau)]$ of the atoms generated by $T_{n'}$. Each of these atoms belong to 3.02 $[(9+2\tau)/(17-8\tau)]$ *XB* clusters in average. Atoms generated

FIG. 11. From left to right: when the cut is translated in $\mathbf{E}_\perp$ glue atoms become part of *B* or $M(M')$ clusters; the clusters rearrange in space through a relatively few number of atom jumps. Observe, on the right, how some glue atoms are arranged in clusters that preclude the formation of either *B* or $M(M')$ clusters.

TABLE IX. Summary of the definitions of the basic clusters and their extensions. The symbol * designates a partial orbit and a bold number designates a full orbit.

Type	Sym(lattice)	6D vector
B **cluster** (origin at *bc*)		
$bc-n$	**12**(*I*)	[3,−1]:(1,1,−1,1,−1,1)/2
$bc-n'$	**20**(*I*)	[3,0]:(−1,1,1,1,1,1)/2
Extended (Duneau)		
$bc-n$	60*(*I*)	[7,−1]:(1,−1,1,1,1,3)/2
$bc-n'$	60*(*I*)	[7,0]:(−1,1,3,−1,−1,−1)/2
$bc-n$	**20**(*I*)	[3,3]:(1,1,1,−1,−1,1)/2
$bc-n'$	**12**(*I*)	[3,4]:(1,1,1,1,−1,1)/2
Next . . .		
$bc-n'$	120*(*I*)	[11,0]:(3,−1,1,−1,−1,3)/2
$bc-n$	60*(*I*)	[7,3]:(−1,1,3,1,1,1)/2
$bc-n'$	60*(*I*)	[7,4]:(−1,3,1,1,−1,1)/2
$bc-n$	60*(*I*)	[11,3]:(3,1,1,−1,−3,1)/2
$bc-n$	60*(*I*)	[11,3]:(1,−1,3,−1,1,3)/2
$bc-n'$	60*(*I*)	[11,4]:(1,−1,3,1,1,3)/2
$bc-n$	**60**(*I*)	[7,7]:(1,1,1,1,−1,3)/2
. . .		
M (*M'*) **cluster** [origin at *n* (*n'*)]		
$n-n'$ $(n'-n)$	20*(*P*)	[6,−3]:(1,0,0,−1,−1,0)
$n-n'$ $(n'-n)$	**12**(*P*)	[2,1]:(0,0,1,0,0,0)
$n-n$ $(n'-n')$	**30**(*F*)	[4,0]:(0,1,0,0,−1,0)
Extended (Duneau)		
$n-n'$ $(n'-n)$	60*(*P*)	[14,−7]:(1,0,−1,1,0,2)
$n-n'$ $(n'-n)$	60*(*P*)	[6,1]:(0,1,0,1,0,1)
Next . . .		
$n-bc$	20*(*I*)	[3,3]:(1,1,1,−1,−1,1)/2
$n-n$ $(n'-n')$	60*(*F*)	[8,0]:(1,0,1,−1,−1,0)
$n'-bc$	12*(*I*)	[3,4]:(1,1,1,1,−1,1)/2
$n-n$ $(n'-n')$	**30**(*F*)	[4,4]:(0,0,1,0,0,1)
$n-n'$ $(n'-n)$	60*(*P*)	[10,1]:(0,0,2,−1,0,0)
$n-n'$ $(n'-n)$	**60**(*P*)	[6,5]:(0,1,1,0,−1,0)
$n-n$	**12**(*F*)	[8,4]:(0,0,2,0,0,0)
$n'-n'$	12*(*F*)	[8,4]:(0,0,2,0,0,0)
$n-n$ $(n'-n')$	60*(*F*)	[8,4]:(1,1,0,0,−1,1)
$n-n'$ $(n'-n)$	60*(*P*)	[10,5]:(1,0,1,−1,−1,1)
$n'-n$	12*(*P*)	[10,5]:(1,1,0,1,−1,1)
. . .		

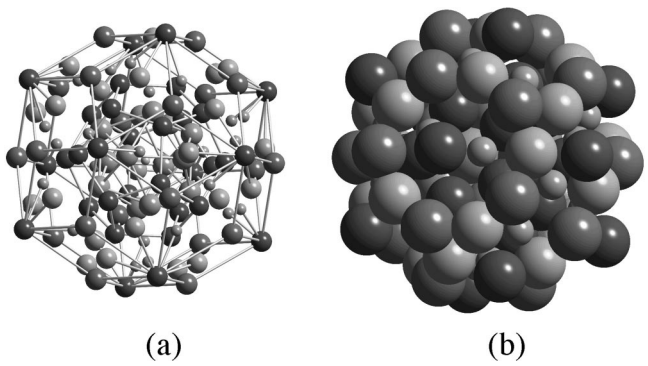

FIG. 12. The extended *XB* cluster proposed by Duneau (Ref. 21) in the complete 112 atoms cluster corresponding to the main configuration (cell C_1 in Table XIII). (a) Balls and sticks view showing the various orbits; (b) space filling view showing in front a large portion of an adjacent *M* cluster.

by $T_{n'}$ never belong simultaneously to a *TI* and a fivefold orbit of the triacontahedron.

The *TI* orbit distributes inside the triacontahedron along threefold directions of the closest atoms of the fivefold orbit of the triacontahedron. The *TI'* orbit distributes on the main diagonal facets of the triacontahedron in the standard τ ratio between the two opposite vertices of the facets. The whole *XB* cluster can be decomposed with the standard set of prolate and oblate rhombohedra of the canonical 3D Penrose tiling with additional atoms decorating some of the facets and threefold axes. We obtain a total of six different decorations of the oblate rhombohedron and 14 of the prolate.

Regrouping the cells generated by all six shells of the *XB* cluster leads to a full covering of the basic atomic surfaces: the *XB* cluster defines a template cluster with an average number of 111.265 $(231-74\tau)$ atoms (ranging from 109 to 112). As already mentioned by Duneau,[21] *any* atom of the structure belongs to one at least such template centered on *bc* site(s) [see Fig. 15(a)].

Performing the complete cell decomposition in projecting all six orbits of atomic surfaces properly located in 6D space onto T_{bc}, leads to the ten cells of Table XIII and shown in

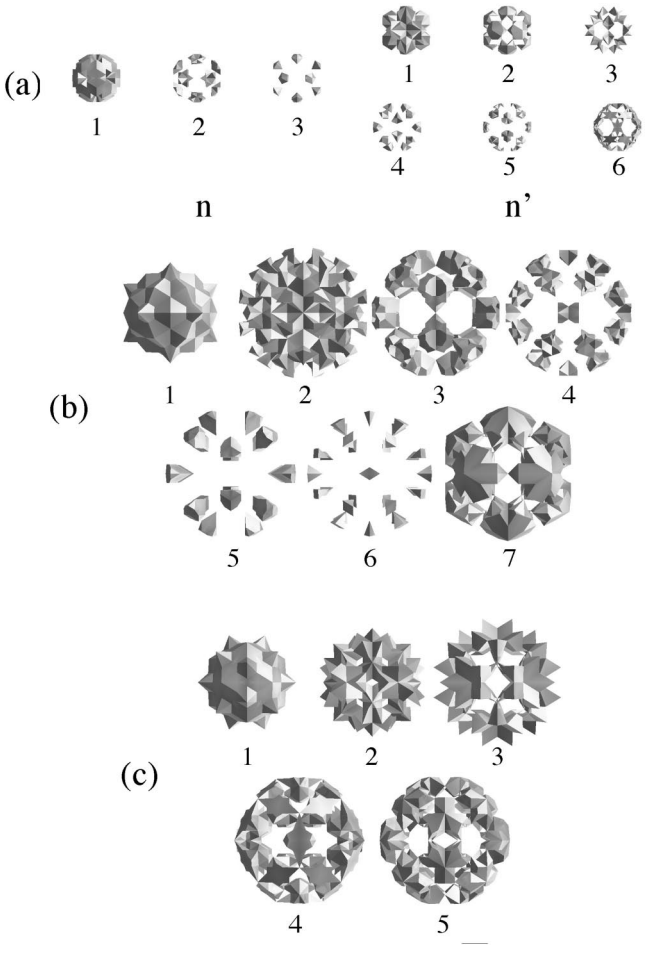

FIG. 13. Cell decompositions of (a) T_{bc}, (b) T_n, and (c) $T_{n'}$ for the two partial *TI*'s orbits of the extended *B* cluster (see Tables X and XI).

TABLE X. Cell decomposition [see Fig. 13(a)] of T_{bc} by T_n at $[7,-1]:(1,-1,1,1,1,3)/2$ and by $T_{n'}$ at $[7,0]:(-1,1,3,-1,-1,-1)/2$ corresponding, respectively, to *TI* and *TI'*.

Cell	Volume	*B*-cluster%	Number of atoms (over 60)
T_n			
C_1	$-25+16\tau$	**88.8544**	24
C_2	$13-8\tau$	5.57281	23
C_3	$13-8\tau$	5.57281	22
$T_{n'}$			
C_1'	$-22+14\tau$	**65.2476**	23
C_2'	$26-16\tau$	11.1456	22
C_3'	$68-42\tau$	4.25725	22
C_4'	$-42+26\tau$	6.88837	21
C_5'	$-110+68\tau$	2.63112	20
C_6'	$81-50\tau$	9.83006	21

TABLE XI. Cell decomposition [see Figs. 13(b) and (c)] of T_n and $T_{n'}$ by T_{bc} complementary to Table X giving the number of *XB* clusters intersecting the atoms of the *TI*'s of a given *XB* cluster.

Cell	Volume	Total at. %	Number of intersecting *XB*'s
T_n			
C_1	$-14+12\tau$	**16.0951**	0
C_2	$55-32\tau$	9.577	1
C_3	$-14+10\tau$	6.479	2
C_4	$23-14\tau$	1.033	3
C_5	$-25+16\tau$	2.640	3
C_6	$-3+2\tau$	0.7015	4
C_7	$-17+14\tau$	**16.797**	2
$T_{n'}$			
C_1'	$11-4\tau$	**13.455**	0
C_2'	$24-14\tau$	4.00	1
C_3'	$-66+42\tau$	5.816	2
C_4'	$10-4\tau$	**10.483**	2
C_5'	$26-14\tau$	9.947	3

TABLE XII. Cell decomposition (see Fig. 14) of T_n and $T_{n'}$ by T_{bc} at, respectively, [3,3]:(1,1,1,−1,−1,1)/2 and [3,4]:(1,1,1,1,−1,1)/2 corresponding to the triacontahedron of the *XB* cluster.

Cell	Volume	Total at. %	Number of intersecting *XB*'s
T_n			
C_1	$36-22\tau$	11.983	7
C_2	$-16+10\tau$	0.5359	6
C_3	$-42+26\tau$	0.2047	6
C_4	$26-16\tau$	0.3312	5
C_5	$-6+4\tau$	14.03	4
C_6	$-16+10\tau$	0.5359	4
C_7	$46-28\tau$	2.065	5
C_8	$-110+68\tau$	0.078	4
C_9	$124-76\tau$	9.00	3
C_{10}	$-66+42\tau$	5.8166	2
C_{11}	$44-26\tau$	5.738	1
C_{12}	$-15+16\tau$	**32.356**	0
$T_{n'}$			
C'_1	$13-8\tau$	0.1656	12
C'_2	$-55+34\tau$	0.0391	10
C'_3	$68-42\tau$	0.1265	9
C'_4	$-42+26\tau$	0.2047	8
C'_5	$13-8\tau$	0.1656	7
C'_6	$-3+2\tau$	0.70149	6
C'_7	$13-8\tau$	0.1656	6
C'_8	$-3+2\tau$	0.70149	5
C'_9	$-6+4\tau$	**14.03**	4
C'_{10}	$46-28\tau$	2.065	3
C'_{11}	$-96+60\tau$	3.215	2
C'_{12}	$69-42\tau$	3.098	1
C'_{13}	$-12+14\tau$	**31.654**	0

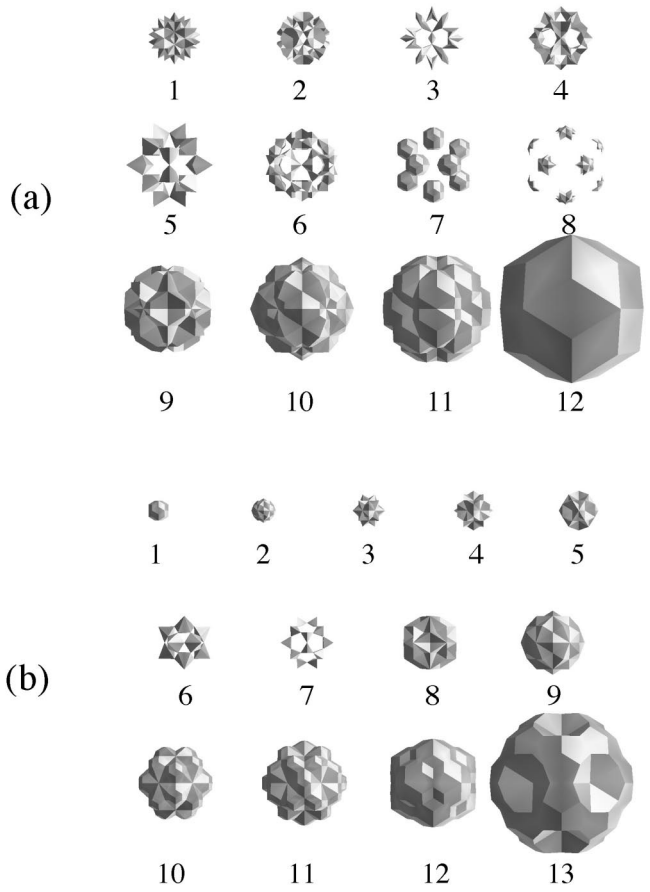

FIG. 14. Cell decompositions of (a) T_n, and (b) $T_{n'}$ for the external (canonical) triacontahedron of the *XB* cluster (see Table XII).

Fig. 15(b). The *XB* cluster has therefore ten different configurations (irrespective of the point symmetry operations), where the most important (with almost 60%), associated to cell C_1, contains the maximum number of 112 atoms. Because it has several configurations this cluster is not a covering cluster *stricto sensu* since its local atomic decoration varies (although these configurations share 109 atoms) from site to site on the two partially *TI* and *TI'* orbits. It is not to be compared with the covering cluster discussed by Gummelt[56] for Penrose tilings. This latter is unique and satisfies specific overlap rules—equivalent to matching rules—that insure the tiling to be quasiperiodic if they are satisfied everywhere. In our present case, the template cluster is not unique and no covering rules, if any, can be deduced from our simple geometrical analysis.

TABLE XIII. Cell decomposition [see Fig. 15(b)] of T_{bc} leading to the ten configurations of the *XB* cluster. Any atom of the structure belongs to one or more of these ten configurations.

Cell	Volume	*XB*-cluster %	Z_{TI}	$Z_{TI'}$	Total number of atoms
C_1	$20-12\tau$	**58.3592**	24	23	112
C_2	$-110+68\tau$	2.63112	23	23	111
C_3	$68-42\tau$	4.25725	22	23	110
C_4	$-42+26\tau$	6.88837	24	22	111
C_5	$-55+34\tau$	1.31556	22	22	109
C_6	$123-76\tau$	2.94169	23	22	110
C_7	$68-42\tau$	4.25725	24	22	111
C_8	$-42+26\tau$	6.88837	24	21	110
C_9	$-110+68\tau$	2.63112	24	20	109
C_{10}	$81-50\tau$	9.83006	24	21	110

IV. DISCUSSION

The present geometrical analysis of the three main atomic clusters *B*, $M(M')$, and *XB* has been derived from the basic fully deterministic model shown in Fig. 1. Models where a fraction of the atomic sites have partial occupancy factors because of too short atom pairs have been proposed that correspond to increasing the size of the atomic surfaces T_n and $T_{n'}$ of Fig. 1.

The first model is due to Elser[16,17] and can be obtained by increasing $T_{n'}$ with small polyhedra (of total volume $-3+2\tau$) at the periphery of the fivefold cups of $T_{n'}$ as shown

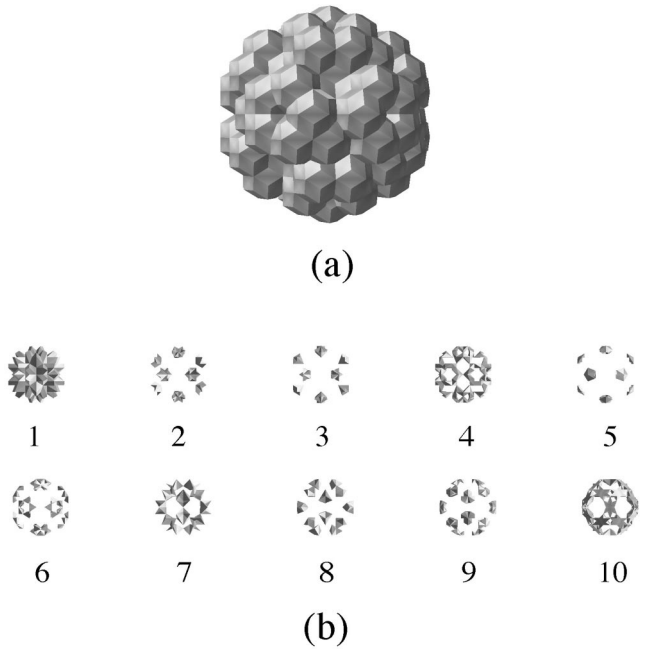

FIG. 15. (a) A portion of the network of XB clusters represented by their external triacontahedra; (b) the complete cell decomposition of T_{bc} defining the existence domains of the ten configurations of the XB cluster (see Table XIII).

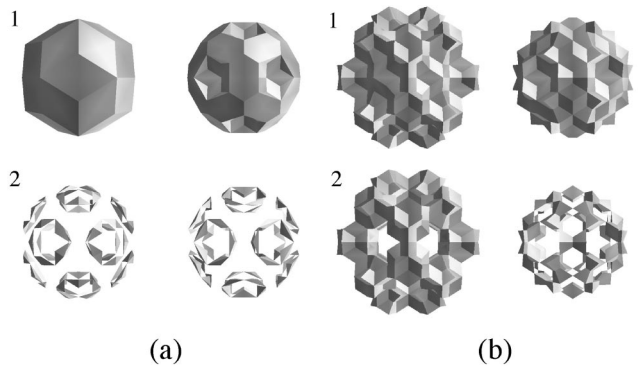

FIG. 16. (a) 1: The simplest atomic surfaces at n and n' consistent with Elser's model (Ref. 16) (after Ref. 20); (a) 2: corresponding overlap regions generating short distances along fivefold directions; (b) 1: the large atomic surfaces of Kramer *et al.* (Ref. 18); (b) 2: corresponding overlap regions generating short distances along both fivefold and twofold directions.

in Fig. 16(a) 1. This leads to an overall volume of $8+16\tau$. This increase in volume generates short distances of length $\sqrt{18-11\tau}$ along the fivefold directions between T_n and $T_{n'}$ so that two new cells appear, shown in Fig. 16(a) 2, with an occupancy factor of 1/2. In Elser's notations, this corresponds to flipping a fraction $-3+2\tau$ of M_2 with M_3 atoms (see Table IV).

The second model, due to Kramer *et al.*[18] and Papadopolos and co-workers[19,20] in a search for decorating oblate and prolate standard rhombohedra of the 3D Penrose tiling consistently with the F character of the 6D lattice. They obtain the atomic surfaces shown on Fig. 16(b) 1 for T_n and $T_{n'}$ of volumes, respectively, $-16+26\tau$ and $-10+16\tau$. These atomic surfaces overlap significantly along fivefold ($T_n/T_{n'}$) and twofold (T_n/T_n and $T_{n'}/T_{n'}$) directions [see Fig. 16(b) 2], thus generating too short distances at, respectively, [18, -11](1,1,-2,1,-1,1) (0.1054 nm for i-AlCuFe) and [20, -12](0,2,-1,0,-2,-1) (0.1793 nm for i-AlCuFe). This implies attributing partial occupancy factors for large portions of the atomic surfaces. The corresponding decomposition is given by Papadopolos and co-workers.[19,20] The remaining parts of the atomic surfaces that have occupancy factor equal to 1 correspond to the external facets of the cells C_2 and C_4' of Fig. 3. These are the definition domains of the B clusters! In other words, the perfectly ordered part of the structure, in this picture, is the network of B clusters and the fivefold orbit of the external triacontahedron of the XB clusters. The other atoms distribute on flipping sites that belong to TI and TI' and a fraction of the threefold orbit of the canonical triacontahedron. Those are mainly atoms belonging to the $M(M')$ clusters. Hence, if we consider the complete set of atomic sites found by Kramer *et al.*[18] as the host atomic network for the F-type structures, we conclude that *the geometric randomization induced by short distance exclusions fully preserves the integrity of the B clusters and is essentially located on the TI and TI′ orbits of the XB cluster*. This is in excellent agreement with the very recent results—published during the writing of the present paper—of Quandt and Elser[57] of *ab initio* calculations for modeling i-AlPdMn: they found the B clusters as the basic dominant elements of the structure.

More generally, B clusters are extremely robust features: *any model based on two main atomic surfaces on n and n′ and a small surface at bc generate B clusters as a natural consequence of the geometry of the 6D lattice.* This distribution of scattering matter in 6D is indeed the main result shared by all the available diffraction data of these structures. Of course, the details of the relative frequencies and connection modes between the clusters depend on the actual shapes of the atomic surfaces, from rather complicated distributions for spherical models down to very simple ones as those obtained here with polyhedral models.

Hence, in summary, these studies all converge to enforce the idea that the F-type icosahedral quasicrystals based on three atomic surfaces at n, n', and bc are best characterized by a network of B clusters attached on the even nodes of a τ-scaled primitive 3D Penrose tiling and connected together by edges (only 1.3% of the B clusters are isolated) rather than a set of isolated or weakly connected $M(M')$ clusters. The B clusters are the center part of the XB clusters that cover the overall structure in ten slightly different configurations of the $TI-TI'$ partial orbits. On the contrary, the $M(M')$ clusters appear as labile entities—especially in their partially occupied inner dodecahedron orbit—and are less significant for characterizing these kinds of structures. To our opinion, the B clusters are definitely the best candidates for identifying the mean structural features of these solids,

for example, those observed on STM high-resolution images of quasicrystalline surfaces. They should also be preferred as guidelines for discussing the microscopic mechanisms of the high-temperature plastic deformation.

ACKNOWLEDGMENTS

We are pleased to thank M. Duneau, P. Kramer, and Z. Papadopolos for many helpful discussions.

[1] A.-P. Tsai, A. Inoue, and T. Masumoto, Jpn. J. Appl. Phys., Part 2 **26**, L1505 (1987).
[2] A.-P. Tsai, A. Inoue, Y. Yokoyama, and T. Masumoto, Mater. Trans., JIM **31**, 98 (1990).
[3] D. Shechtman, I. Blech, D. Gratias, and J.W. Cahn, Phys. Rev. Lett. **53**, 1951 (1984).
[4] *The Physics of Quasicrystals*, edited by P.J. Steinhardt and S. Ostlund (World Scientific, Singapore, 1987).
[5] *Aperiodicity and Order Series*, edited by M.V. Jarić (Academic Press, New York, 1988-1989).
[6] *Quasicrystals: A Primer*, edited by C. Janot (Oxford Science Publications, 1992).
[7] *Lectures on Quasicrystals*, edited by F. Hippert and D. Gratias (Les Éditions de Physique, Les Ulis, 1994).
[8] M. Cornier-Quiquandon, A. Quivy, S. Lefebvre, E. Elkaim, G. Heger, A. Katz, and D. Gratias, Phys. Rev. B **44**, 2071 (1991).
[9] M. Boudard, M. de Boissieu, C. Janot, J.M. Dubois, and C. Dong, Philos. Mag. Lett. **64**, 197 (1991).
[10] M. Cornier-Quiquandon, R. Bellissent, Y. Calvayrac, J.W. Cahn, D. Gratias, and B. Mozer, J. Non-Cryst. Solids **153&154**, 10 (1993).
[11] M. Boudard, M. de Boissieu, C. Janot, G. Heger, C. Beeli, H.U. Nissen, H. Vincent, M. Audier, and J.M. Dubois, J. Non-Cryst. Solids **153**, 5 (1993).
[12] M. de Boissieu, P. Guyot, and M. Audier, in *Lectures on Quasicrystals* (Ref. 7), pp. 1, 152.
[13] A. Katz and D. Gratias, J. Non-Cryst. Solids **153-154**, 187 (1993).
[14] E. Cockayne, R. Phillips, X.B. Kan, S.C. Moss, J.L. Robertson, T. Iskimaza, and M. Mori, J. Non-Cryst. Solids **153-154**, 140 (1993).
[15] A. Katz and D. Gratias, in *Proceedings of the 5th International Conference on Quasicrystals*, edited by C. Janot and R. Mosseri (World Scientific, Singapore, 1995), pp. 164, 167.
[16] V. Elser, Philos. Mag. B **73**, 641 (1996).
[17] V. Elser, in *Proceedings of the 6th International Conference on Quasicrystals*, edited by S. Takeuchi and T. Fujiwara (World Scientific, Singapore, 1998), pp. 19, 26.
[18] P. Kramer, Z. Papadopolos, and W. Liebermeister, in *Proceedings of the 6th International Conference on Quasicrystals* (Ref. 17), pp. 71, 76.
[19] Z. Papadopolos, P. Kramer, W. Liebermeister, in *Proceedings of the International Conference on Aperiodic Crystals*, edited by M. de Boissieu, J.-L. Verger-Gaugry, and R. Currat (World Scientific, Singapore, 1997), pp. 173–181.
[20] Z. Papadopolos, P. Kramer, G. Kasner, and D.E. Bürgler, in *Quasicrystals*, edited by J.-M Dubois, P.A. Thiel, A.-P. Tsai, and K. Urban, MRS Symposia Proceedings No. 553 (Materials Research Society, Pittsburgh, 1999), pp. 231–236.
[21] M. Duneau, Clusters in Quasicrystals, in Proceedings of the 7th International Conference on Quasicrystals, Stuttgart, September 1999 (in press).
[22] P. Guyot and M. Audier, Philos. Mag. B **52**, L15 (1985).
[23] V. Elser and C.L. Henley, Phys. Rev. Lett. **55**, 2883 (1985).
[24] G. Bergman, L.T. Waugh, and L. Pauling, Acta Crystallogr. **10**, 254 (1957).
[25] A.L. Mackay, Acta Crystallogr. **15**, 916 (1962).
[26] A. Janner and T. Janssen, Phys. Rev. B **15**, 643 (1977).
[27] M. Duneau and A. Katz, Phys. Rev. Lett. **54**, 2688 (1985).
[28] P.A. Kalugin, A.Y. Kitayev, and L.S. Levitov, Pis'ma Zh. Éksp. Teor. Fiz. **41**, 119 (1985) [JETP Lett. **41**, 145 (1985)].
[29] P.A. Kalugin, A.Y. Kitayev, and L.S. Levitov, J. Phys. (France) Lett. **46**, L601 (1985).
[30] P. Bak, Phys. Rev. B **32**, 5764 (1985).
[31] A. Katz and M. Duneau, J. Phys. (France) **47**, 181 (1986).
[32] V. Elser, Acta Crystallogr., Sect. A: Found. Crystallogr. **A42**, 36 (1986).
[33] P. Bak, Scr. Metall. **20**, 1199 (1986).
[34] P. Bak, Physica B & C **136**, 296 (1986).
[35] T. Janssen, Acta Crystallogr., Sect. A: Found. Crystallogr. **A42**, 261 (1986).
[36] T. Janssen, Acta Crystallogr., Sect. A: Found. Crystallogr. **A47**, 243 (1991).
[37] J.W. Cahn, D. Shechtman, and D. Gratias, J. Mater. Res. **1**, 13 (1986).
[38] J. Conway, quoted in M. Gardner, ''Metamathematical Games,'' Sci. Am., January (1977).
[39] M. Kléman and P. Pavlovitch, J. Phys. (Paris), Colloq. **47**, C3-229 (1986).
[40] L.S. Levitov, Commun. Math. Phys. **119**, 627 (1988).
[41] A. Katz, Commun. Math. Phys. **118**, 263 (1988).
[42] J.E.S. Socolar, Commun. Math. Phys. **129**, 599 (1990).
[43] F. Gähler, J. Non-Cryst. Solids **153&154**, 160 (1993).
[44] D. Frenkel, C.L. Henley, and E.D. Siggia, Phys. Rev. B **34**, 3649 (1986).
[45] P.A. Kalugin and L.S. Levitov, Int. J. Mod. Phys. B **3**, 877 (1989).
[46] A. Katz, in *Introduction to the Mathematics of Quasicrystals*, Aperiodicity and Order Vol. 2, edited by M.V. Jarić (Academic Press, New York, 1989), pp. 53, 79.
[47] A. Katz, in *Proceedings of the Anniversary Adriatico Research Conference on Quasicrystals*, edited by M. Jarić and S. Lundqvist (World Scientific, Singapore, 1990), pp. 200, 217.
[48] A. Katz and D. Gratias, in *Lectures on Quasicrystals* (Ref. 7), pp. 187, 264.
[49] C. Janot and M. de Boissieu, Phys. Rev. Lett. **72**, 1674 (1994).
[50] M. Audier, P. Sainfort, and B. Dubost, Philos. Mag. B **54**, L105 (1986).
[51] M. Audier, J. Pannetier, M. Leblanc, C. Janot, J.-M. Lang, and B. Dubost, Physica B **153**, 136 (1988).

[52] C. Oguey, M. Duneau, and A. Katz, Commun. Math. Phys. **118**, 99 (1988).
[53] P. Kramer, J. Math. Phys. **29**, 516 (1988).
[54] V.I. Arnol'd, Physica D **33**, 21 (1988).
[55] S. Lyonnard, G. Coddens, Y. Calvayrac, and D. Gratias, Phys. Rev. B **53**, 3150 (1996).
[56] P. Gummelt, in *Proceedings of the 5th International Conference on Quasicrystals* (Ref. 15), p. 84; Geom. Dedicata **62**, 1 (1996).
[57] A. Quandt and V. Elser, Phys. Rev. B **61**, 9336 (2000).